



**International Journal of Global Energy Issues**

ISSN online: 1741-5128 - ISSN print: 0954-7118

<https://www.inderscience.com/ijgei>

---

**Smart plant propagation algorithm for the improvement of self-excited induction generator performance**

Swati Paliwal, Sanjay Kumar Sinha, Yogesh Kumar Chauhan

**DOI:** [10.1504/IJGEI.2023.10053981](https://doi.org/10.1504/IJGEI.2023.10053981)

**Article History:**

Received:	13 April 2022
Last revised:	28 September 2022
Accepted:	21 November 2022
Published online:	03 December 2023

---

## Smart plant propagation algorithm for the improvement of self-excited induction generator performance

---

Swati Paliwal\* and  
Sanjay Kumar Sinha

Department of Electrical and Electronics Engineering,  
Amity University,  
Noida, Uttar Pradesh, India  
Email: swatipaliwal03@gmail.com  
Email: sksinha6@amity.edu  
\*Corresponding author

Yogesh Kumar Chauhan

Department of Electrical Engineering,  
Kamla Nehru Institute of Technology,  
Sultanpur, Uttar Pradesh, India  
Email: chauhanyk@yahoo.com

**Abstract:** India has taken effective initiatives to generate a massive amount of electrical power from wind energy. In order to strengthen the development of offshore wind power, self-excited induction generators (SEIG) have proven to be the best choice. But the global acceptance of this machine depends on its improved voltage and frequency regulation. Therefore, this work investigates the performance of SEIG in short and long shunt configurations under different loading conditions and at different power factors. This paper employs one of nature's most unique and inspired techniques, Plant Propagation Algorithm (PPA), to improve machine performance in terms of flux or voltage. The PPA is based on the propagation strategy of the strawberry plant, which has the potential to colonise new areas in pursuit of better survival chances. From simulated results, it has been observed that the short shunt configuration requires lower shunt and series capacitance in order to improve SEIG performance.

**Keywords:** self-excited induction generator; plant propagation algorithm; Newton Raphson method; loading conditions; simulated annealing; wind energy conversion system; machine flux or voltage.

**Reference** to this paper should be made as follows: Paliwal, S., Sinha, S.K. and Chauhan, Y.K. (2024) 'Smart plant propagation algorithm for the improvement of self-excited induction generator performance', *Int. J. Global Energy Issues*, Vol. 46, Nos. 1/2, pp.137–156.

**Biographical notes:** Swati Paliwal is pursuing her PhD degree from Amity University Noida, UP. Currently, she is working at Mahatma Gandhi Institute of Technology in Hyderabad as an Assistant Professor. Her research interests include power systems and SEIG.

Sanjay Kumar Sinha obtained BE degree (M.I.T Muzaffarpur), MTech degree (NIT Jamshedpur) and PhD degree (IIT Roorkee), respectively. Presently, he is working as a Professor in the Department of Electrical and Electronics Engineering at Amity University Noida, UP. His research interests include electrical engineering and power system.

Yogesh Kumar Chauhan obtained BTech degree (GBPU Pant Nagar), MTech degree (IIT, Delhi) and PhD degree (TU, Patiala) in 1997, 1998 and 2010, respectively. He worked as a Faculty Member in EIED, TU, from February 2000 to January 2011. Presently, he is working as an Associate Professor in the Department of Electrical Engineering at Kamla Nehru Institute of Technology. His research interest includes power converters, drives and SEIG.

---

## 1 Introduction

The widespread and devastating effects of climate change caused by anthropogenic activities have compelled the world to utilise environmentally friendly sources of energy generation. In order to meet the international goal of limiting the average rise in global temperature to 1.5°C, it is important to limit carbon emissions to ensure sustainable growth in the world. India has been rolling out various initiatives, policies and incentives to accelerate renewable power generation to pursue its low carbon emission goals. Among other renewable energy sources, wind energy has shown consistent progress in decentralised areas (MNRE report 2020–2021, Government of India). India also has tremendous offshore wind power generation potential. Considering this, the government has notified the policy for offshore power generation. The latest assessment by NIWE indicates that the gross wind potential in India is about 302.25 GW at 100 metres above the ground level (MNRE data). With the establishment of the wind sector, various state-of-the-art machineries such as PMSG, DFIG, SCIG and SEIG, have evolved.

To achieve power generation from wind, especially at offshore locations, it is preferable to use SEIG (Benhacine et al., 2021). SEIG is an externally driven induction generator along with a capacitor bank to provide proper excitation. Based on various criteria, the minimum and maximum values of capacitance and speed have been chosen for the successful operation of SEIG under different loading conditions. It offers advantages over synchronous generators, like reduced cost, a brushless rotor, easy maintenance and the absence of separate DC sources. But the resulting EMF and current would continue to increase indefinitely until magnetic saturation is reached (Kalla et al., 2021). The external shunt capacitance, magnetising characteristic, Prime Mover (PM) speed and load all influence the SEIG terminal voltage. The capacitor bank provides SEIG with the required Volt-Amp Reactive (VAR). The terminal voltage drops as the generator is loaded from no load to full load due to a mismatch between the VAR requested by the generator and the VAR supplied by the capacitor bank (Krishna and Sandeep, 2022). This results in a major lacuna in its application (Khan et al., 2017). But it has wide applications in pico/mini hydropower generation, chemical companies and refineries. This variety of nonlinear loads leads to high inrush current, voltage fluctuations and power factor reduction. The results of this non-linearity lead to overheating, insulation stress, winding stress and vibration in the shaft. As a result, SEIG's global acceptance is contingent on strategies that address its flaws and its ability

to handle dynamic loads under unbalanced conditions. Therefore, the main concentration in recent years has shifted to improving the voltage and frequency regulation of SEIG. In Aberbour et al. (2020) and Al-Senaidi et al. (2021), mathematical modelling of SEIG has been performed in terms of magnetic saturation, cross-saturation and the effect of iron losses by using series compensation to improve its accuracy.

Various voltage regulating schemes like switched capacitors, variable inductors, saturated reactors and other semi-conductor-based devices have been implemented in SEIG (Chaturvedi, 2022; Teng et al., 2019; Ali et al., 2019; Esmeel, 2020). The complex control circuit of the voltage regulator and other problems like harmonics and associated transients make it inefficient to use. Hence, the short-shunt and long-shunt configurations of SEIG have been employed to reduce the voltage regulator's complexity (Chaturvedi and Goel, 2019). The short and long shunt configurations depend on the series capacitor's placement in the SEIG machine. In Khan et al. (2022), the dynamic response of short and long-shunt SEIG connected with an induction motor load has been discussed. Similarly, Esquivel-Sancho et al. (2021) and Chaturvedi et al. (2020) discussed steady-state modelling of short and long-shunt SEIG to improve flux using the optimum capacitance value.

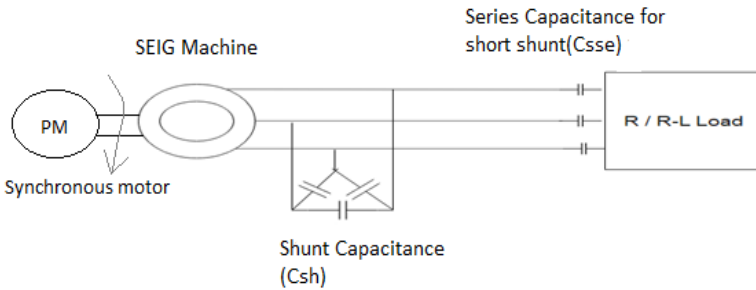
Saha and Sadhu (2018), Sathpathy et al. (2019) and Mohiudin and Sharma (2021) discussed the magnetising reactance and frequency of SEIG, identified using an iterative procedure and established the correlation between the various computational algorithms and the experimental results. Three optimisation techniques named GA, PSO and SA have been used to optimise the values of magnetising reactance and frequency, respectively (Hannaan et al., 2018; Bouhadjra et al., 2020). The optimisation is performed on the SEIG feeding the resistive load. GA has been used to improve SEIG performance (Dewangan et al., 2019; Varshney et al., 2021). Paliwal et al. (2019) used GSA in the frequency improvement of the machine. SEIG performance becomes sluggish because the frequency and magnetising reactance change with load, even at constant rotor speed. Therefore, three constraints are necessary for SEIG machine modelling (e.g., Equality, Inequality and Bound Limits) (Khan et al., 2022). Therefore, steady-state analysis is required to obtain the required parameters to increase its effectiveness. In order to model an equivalent circuit and compute an objective function, it is important to understand the block diagram and steady-state equivalent circuit diagram discussed in the mathematical modelling section.

The literature outlined above mainly focuses on voltage and frequency regulation due to uncertainties in voltage and frequency in the wind turbine-driven SEIG. Many optimisation techniques like Fuzzy controller, GA and GSA have been used, but no work has been recorded on plant propagation algorithms serving induction machines' performance. Therefore, in this paper, a 3-phase, 3kW, 415 V, 10 A (line) machine has been used as a SEIG machine, as mentioned in Appendix A.1. And its performance and loadability have been improved in terms of flux ( $V/f$ ) by using an optimised value of capacitance and speed. These optimised parameters of the steady state equivalent circuit have been obtained using the plant propagation algorithm. The simulated results at different loading conditions and at different power factors for short and long shunt configurations have also been considered in this paper and are shown in the result and discussion section. The paper is outlined as follows: an introduction, mathematical modelling, an optimisation technique, results & discussion and a conclusion.

## 2 Mathematical modelling

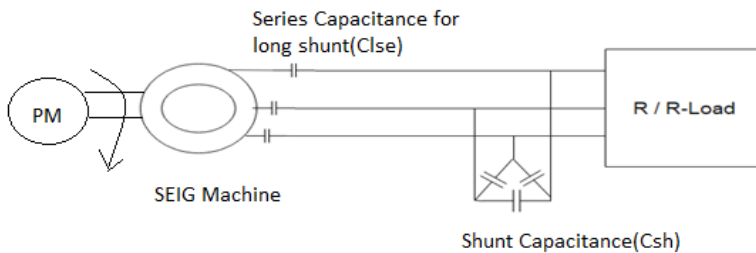
An EMF is induced in the machine windings if a suitable three-phase capacitor bank is placed across an externally powered induction motor. In the SEIG machine, a steady increase in capacitor VAR with load is required to achieve good voltage regulation. Figures 1 and 2 represent the schematic diagram of the short and long shunt SEIG, respectively; here,  $C_{sh}$  is defined as shunt capacitance selected to provide no load voltage. And  $C_{lse}$  and  $C_{sse}$  are defined as series capacitance for the long and short shunt models, respectively, which is selected to provide the required voltage/frequency regulation at full load.

**Figure 1** Schematic diagram of short shunt SEIG



The difference between short shunt and long shunt configuration is the placement of a series capacitor in the machine. A series capacitor connected near the load side is named a short shunt SEIG, as shown in Figure 1. Figure 2 shows a series capacitor connected near the prime mover side as a long shunt SEIG. The selection of capacitance plays an important role in the performance analysis of SEIG. Hence, it is important to optimise capacitance value using artificial intelligence. The purpose of capacitance is to provide stable operation of the SEIG machine connected with a variable load ( $R/RL$ ).

**Figure 2** Schematic diagram of long shunt SEIG



Three constraints are required to model the SEIG machine, viz. Equality, Inequality and Bound Limits. Since frequency ( $f$ ) and magnetising reactance ( $X_m$ ) vary with the load even at constant rotor speed, SEIG performance becomes sluggish. In order to improve its performance, steady state analysis is required to determine the required parameters. Since the  $V/f$  ratio is proportional to flux, any change in flux will result in increased

system loss. Hence, this paper provides a bound limit of 15% so that  $V/f$  operates within a limited range.

Here,

- $X_{sh}$  : Shunt capacitive reactance in ohm
- $X_{lse}$  : Series capacitive reactance for a long shunt in ohm
- $X_{sse}$  : Series capacitive reactance for a short shunt in ohm
- $X_s$  : Leakage reactance of stator winding in ohm
- $X_L$  : Inductive reactance of load in ohm
- $X_m$  : Magnetising reactance in ohm
- $X_r$  : Leakage reactance of rotor winding in ohm
- $V_g$  : Generated voltage in per unit
- $V_l$  : Load voltage in per unit
- $R_s$  : Stator resistance in ohm
- $R_L$  : Load resistance in ohm
- $R_r$  : Rotor resistance in ohm
- $n$  : Per unit speed
- $f$  : Per unit frequency
- $I_L$  : Load current in ampere
- $I_c$  : Capacitor current in ampere
- $Z_L$  : Load Impedance in ohm

The majority of approaches for evaluating the steady-state effectiveness of SEIG in the literature require the separation of the real and imaginary components of the complex impedance. If the machine's core loss is also considered, the model becomes much more difficult. Figure 3 represents the steady state circuit where  $R_s$  and  $X_s$  are resistance and leakage reactance at the stator side, respectively, whereas  $R_r$  and  $X_r$  are the resistance and leakage reactance at the rotor side, respectively. Under self-excitation, the loop equation of the equivalent circuit is given by:

$$Z_{eq} * I_{QP} = 0 \quad (1)$$

$$Z_{eq} = Z_1 (C_{sh}, C_{sse}/C_{lse}, X_m, F) + jZ_2 (C_{sh}, C_{sse}/C_{lse}, X_m, F) \quad (2)$$

Loop impedance  $Z_{eq}$  formulates the equality constraints using equation (2).

$Z_1$  and  $Z_2$  at 'A-th' load are expressed in terms of coefficients, defined in Appendix A.2.

$$Z_{1,A} = \sum_{n=0}^3 (P_A^{2n+1} + P_A^{2n+2} X_{m,A}) F_A^n = 0 \quad (3.A)$$

$$Z_{2A} = \sum_{n=0}^3 (Q_A^{2n+1} + Q_A^{2n+2} X_{m,A}) F_A^n = 0 \tag{3.B}$$

Coefficients of  $P$  and  $Q$  are expressed in Appendix B and are solved by Newton Raphson (NR) method.

$$Z_{PR} = \left( Z_L - j \frac{X_{sse}}{f_{pu}} \right) \parallel \left( -j \frac{X_{sh}}{f_{pu}} \right) \tag{4}$$

$$Z_{PQ} = \frac{R_s}{f_{pu}} + \frac{R_r f}{(f-v)} + j \left( X_s + \frac{X_r}{2} - \frac{X_{lse}}{f_{pu}} \right) \tag{5}$$

$$Z_{eq} = Z_{PR} + Z_{PQ}$$

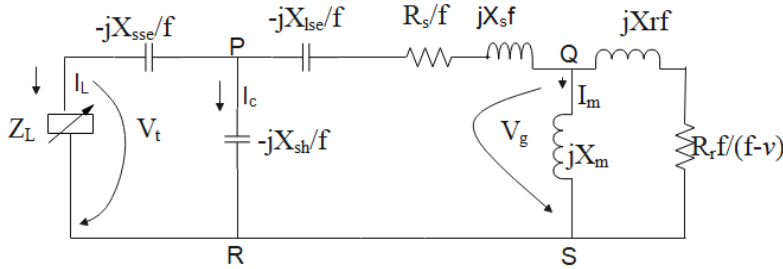
$$I_{QP} = \left( \frac{V_g}{f_{pu}} \right) / Z_{eq} \tag{6}$$

$$I_L = -jX_{sh} * \frac{I_{QP}}{\left[ Z_L f_{pu} - j(X_{sse} + X_{sh}) \right]} \tag{7}$$

$$V_t = I_L * Z_L \tag{8}$$

$$Power = I_L^2 R_L \tag{9}$$

**Figure 3** Steady-state equivalent circuit of SEIG



Equations (4) to (9) expressed the equivalent circuit modelling of SEIG, which has been solved using the Newton-Raphson method.

Equation (10) expressed the objective function to achieve  $V/f$  regulation in speed, magnetising reactance, shunt capacitance and series capacitances, respectively.

$$F_{obj} (n, X_m, C_{sh}, C_{sse}/C_{lse}) = \frac{1}{SP} \sum_{r=0}^{SP} \left\{ \frac{\left[ \frac{V \ln}{f} (n, X_m, C_{sh}, C_{sse}/C_{lse}) \right] - \left[ \frac{Vr}{fr} (n, X_m, C_{sh}, C_{sse}/C_{lse}) \right]}{\frac{Vr}{fr}} \right\}^2 \tag{10}$$

$$F_1 = \frac{1}{F_{obj}(n, X_m, C_{sh}, C_{sse}/C_{lse})} \quad (11)$$

$F_{obj}$  is the mean squared mismatch between load flux and rated flux from no load-to-load point. The minimum fitness of equation (10) is expressed using fitness  $F_1$  in equation (11). The optimum fitness of objective function has been obtained using the PPA approach. In addition to performance, loadability, defined as machine loading capacity, is expressed as fitness  $F_2$  in equation (12).

$$F_2 = \frac{Pl}{Pr} \quad (12)$$

where  $Pl$  is the output power per unit

$Pr$  is the rated power per unit

### 3 Plant propagation algorithm

Optimisation problems in electrical engineering consist of non-linear loads, constraints and many other discrete variables. Therefore, heuristic procedures are being used to find feasible solutions. But a heuristic approach leads to too many limitations like stochasticity, limited theory support and undefined parameters. The success rate of nature-inspired algorithms in nonlinear problems is particularly notable compared to classical optimisation approaches. In the 17th century in Paris, Amedee-Francois Frezier, a mathematician and engineer, brought some Chilean strawberry plants that produced large strawberry fruits (Salhi and Eric, 2017). The strawberry plant belongs to the rose family and can colonise new territories for favourable survival. The strawberry plant metaheuristic approach inspired Plant Propagation Algorithm (PPA). As a result of crossing and selection, the strawberry plant industry grows. If the ground spot is good with all nutrients and light, it will send short runners that give new strawberry plants and occupy the neighbourhood as best they can. If the ground spot is not good, it will send a few runners to find a better spot for its new offspring (Almazini et al., 2022). PPA is tested on the standard test function of chlorobenzene purification having non-linear behaviour and is compared with the Nelder-Mead algorithm (Salhi and Eric, 2017). Sulaiman et al. (2018) used the PPA approach to handle optimisation problems involving constraints and found it superior to other nature-inspired optimisation techniques.

PPA optimisation also follows a few assumptions, which are as follows:

- a) For a poor spot of plant, the long runner is avoided.
- b) The quality of the spot is directly proportional to the plant's growth.

Consider what a strawberry plant, and indeed any plant reproduces by sending out runners, will do to increase its chances of surviving. It is acceptable to suppose that there is little pressure on it to leave that position on the earth if it is in a good spot with access to enough water, nutrients and light to ensure its survival. The mother plant will search for a better location for its offspring if, on the other hand, it is in a location that is deficient in water, nutrients, light or any other factor needed for a plant to live. It will

therefore send a few runners farther out to investigate far-off neighbourhoods. Since sending a long run is a significant investment for a plant in a bad location, it is reasonable to predict that it will only send a few numbers. It can be further supposed that the plant's growth reflects the spot's quality (ample nutrients, water and sunshine). With these assumptions, in this paper optimised value of capacitances required in the performance analysis of SEIG has been calculated using the PPA approach and is described as follows:

Let us consider that a plant  $P_i$  is in spot  $C_i$  in dimension 'S', and 'SP' is the number of strawberry plants initially (load points) or population size, maximum generations  $g_{max}$  and maximum number optimum runners  $S_{max}$  per plant.

where

$$C_i = \{C_{i,j}; \text{ for } j = 1 \dots S\} \tag{13}$$

The generalised PPA code for multi-objective functions is defined by Sulaiman et al. (2018). This paper's objective function is to have optimum mean square voltage /frequency regulation and loadability. In doing so, different plant positions are normalised in terms of  $S_i$  to rank them as a fitness function. The pseudo-code for the SEIG machine using the Newton Raphson method and optimised PPA technique is mentioned below and explained using a flowchart.

### 3.1 PPA pseudo code for SEIG

#### 1. Initialisation of $Fobj$ (Mean square mismatch for flux)

$g_{max} \leftarrow$  Maximum number of iterations(generation);  $SP \leftarrow$  Population size =30 for 3 kW rated motor capacity;  $q \leftarrow$  trail run

global  $pufmn$   $pufmx$   $Xmmn$   $Xm mx$  % per unit minimum frequency, maximum frequency, per unit minimum magnetising reactance, maximum magnetising reactance%

global  $ismx$   $Vl mn$   $Vl mx$  %Maximum stator current, Load voltage minimum in per unit, Load voltage maximum%

% The maximum and minimum frequencies are 10% higher and lower than the rated frequency, respectively.  $ismx = 1.1$  p.u,

$$Vl mx = 0.92 \text{ p.u, } Vl mx = 1.08 \text{ p.u\%}$$

#### 2. if $q \leq SP$ then

#### 3. Generate population of capacitance ( $COPg$ ) (Short shunt and long shunt values)

$COPg = \{C_{i,j}; \text{ for } i = 1, 2, \dots, SP\}$  using equation (2) and gather best solution

$$20\mu F \leq Csh \leq 40\mu F,$$

$$50\mu F \leq Csse \leq 250\mu F,$$

$$200\mu F \leq Clse \leq 600\mu F,$$

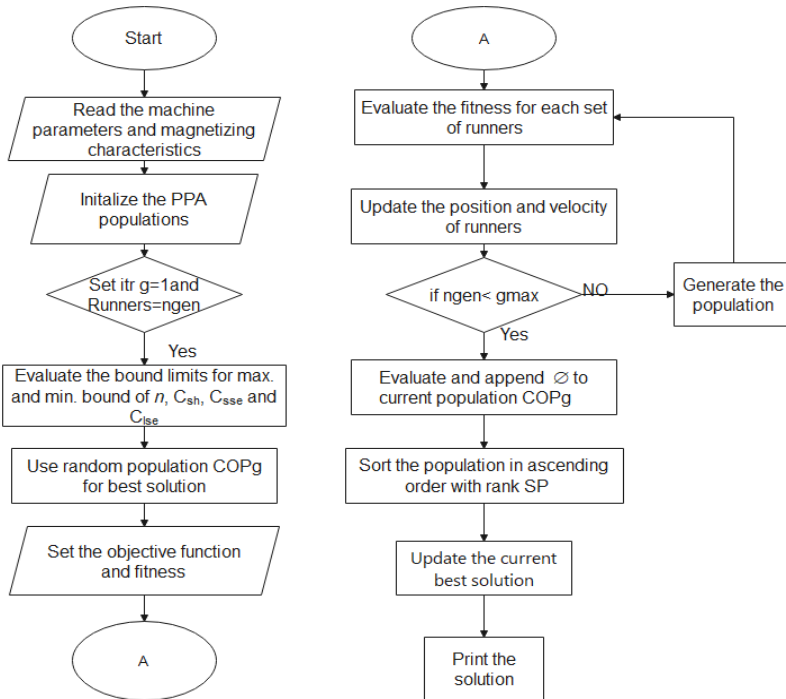
$0.88 pu \leq n \leq 1.12 pu$   
 $nmu = 160$                       %  $nmu$  = no of points generated for p.u speed  
 $ncsh = 160$                       %  $ncsh$  =no of points generated for p.u shunt capacitor  
 $ncss = 160$                       %  $ncss$  =no of points generated for p.u series capacitor

4. **end if**
5. **while**  $q > SP$  **do**
6. Utilise best solutions from previous runs named  $COPg$
7. function [fitness]=fit\_fun(nucsh0)
- Calculate fitness for each column  $j$  of  $COPg$
8. **end while**
9. Evaluation of population ( $Sm$ ).
10. Choose number of runners,  $nT = 3$ ,  $ngen = 1$ , where  $ngen$  is the no. of generated runners
11. **While** ( $(ngen < g_{max})$ ) **do**
12. Create  $\emptyset$ :
13. **for**  $i=1$  to  $SP$ , **do**
14.   **for**  $k=1$  to  $nT$  **do**
15.     **if**  $q \leq SP$  **then**
16.       **if**  $rand \leq Sm$  **then**
17.          Generate a new solution  $X^*$  according to equation (10), evaluate and store it in  $\emptyset$ ;
18.           **end if**
19.       **if**  $rand \leq Sm$  **then**
20.           $fitness = 1 / (1 + Fobj)$                       % Minimisation of objective function%
- Generate a new solution  $X^*$  according to equation (11), evaluate and store it in  $\emptyset$ ;
21. **else**
22.   fitness=0
23.     **end if**
24.   **else**
25.     **for**  $j=1:n$  **do**
26.       **if** ( $fitness_j < 5$ ) **or** ( $rand \leq Sm$ ) **then** update  $j$ -th entry of  $C_i$  for  $i=1, 2, \dots, SP$  according (2)
27.       **end if**
28.       Evaluate new solution  $X^*$  and store it in  $\emptyset$ ;
29.     **end for**
30.   **end if**

- 31. **end for**
- 32. Add  $\emptyset$  to current population;
- 33. Sort the population in ascending order for objective function %  
Objective function is  $V/F$  regulation%
- 34. Update the current best; % Current best of speed and capacitance%
- 35. **end while**
- 36. **Return:** Optimised Population.

The step-by-step procedure of the PPA algorithm in the SEIG machine, using the Newton Raphson method, has been formulated along with a flowchart, as shown in Figure 4. The flowchart initialises magnetising parameters, evaluating population size and optimisation using the best runner. Here, population consists of shunt and series capacitance along with speed. Population size will design the runner count and evaluate fitness. As mentioned above, this paper’s objective function is flux and loadability control. The mentioned fitness has been evaluated under equality, inequality and bound limits. PPA will search for the best possible runners with rank SP (load points) based on given data. And accordingly updates the position and velocity to find the best solutions.

**Figure 4** Flowchart of PPA algorithm in SEIG



## 4 Results and discussion

The work in results and discussion illustrates the simulated results for the 3-phase, 3 kW, 415 V, 10 A SEIG machine. The characteristics of SEIG are obtained with continuous variation in load without loss of excitation.

Tables 1 and represent the summary of the optimum power output for  $R$  and  $R-L$  load in short and long shunt SEIG, respectively. In the short shunt configuration,  $Clse$  is kept equal to 0. The optimum point (optimum fitness) is obtained at a speed of 1.01  $pu$  slightly higher than the rated speed of 1  $pu$  in a short shunt for  $R$ -load. In contrast, it is obtained at a speed of 0.96  $pu$  slightly lower than the rated speed in  $R-L$  load for the same configuration shown in Table 2. Therefore, it has been concluded that the fitness value is better in  $R$ -load than in  $R-L$  load, which is further verified by its characteristics. The drawn performance characteristic of SEIG has been shown in Figure 5 for  $R$ -load. In Figure 5, it is considered that  $Csh = 30.21 \mu f$  and  $Csse = 205.33 \mu f$ . The addition of  $Csse$  results in better-overloaded capability. The result shows a no-load terminal voltage of 1.01  $pu$  (base voltage of 230 V). It is also observed from Figure 5 that no load voltage with output power is showing marginal progress. With the increase in load,  $Vt$  increases to 1.01  $pu$  and  $Vl$  decreases to 0.962  $pu$ , whereas  $Is$  increases from 0.386  $pu$  to 1.075  $pu$ .

**Table 1** Summary of optimum power output for resistive load

$n$ ( $pu$ )	$Csh$ ( $\mu F$ )	$Csse$ ( $\mu F$ )	$Clse$ ( $\mu F$ )	$Pout$ ( $pu$ )	$R$ Load
1.00	21.35	198.00	–	0.82	Short Shunt
1.01	20.21	201.36	–	0.85	
1.04	23.47	195.85	–	0.79	
1.05	24.00	176.97	–	0.68	
1.00	22.53	–	221.22	0.75	Long Shunt
1.03	21.36	–	239.52	0.78	
1.04	24.76	–	220.01	0.65	
1.05	24.89	–	195.84	0.59	

**Table 2** Summary of optimum power output for resistive-inductive load

$n$ ( $pu$ )	$Csh$ ( $\mu F$ )	$Csse$ ( $\mu F$ )	$Clse$ ( $\mu F$ )	$Pout$ ( $pu$ )	$R-L$ Load
1.00	23.82	192.22	–	0.74	Short Shunt
0.96	22.33	202.32	–	0.79	
0.92	24.00	198.52	–	0.69	
0.89	24.65	182.66	–	0.64	
0.85	23.56	–	247.61	0.72	Long Shunt
0.90	24.54	–	230.26	0.74	
0.82	26.31	–	211.87	0.63	
0.73	26.87	–	198.98	0.60	

**Figure 5** Performance characteristics of short shunt SEIG (see online version for colours)

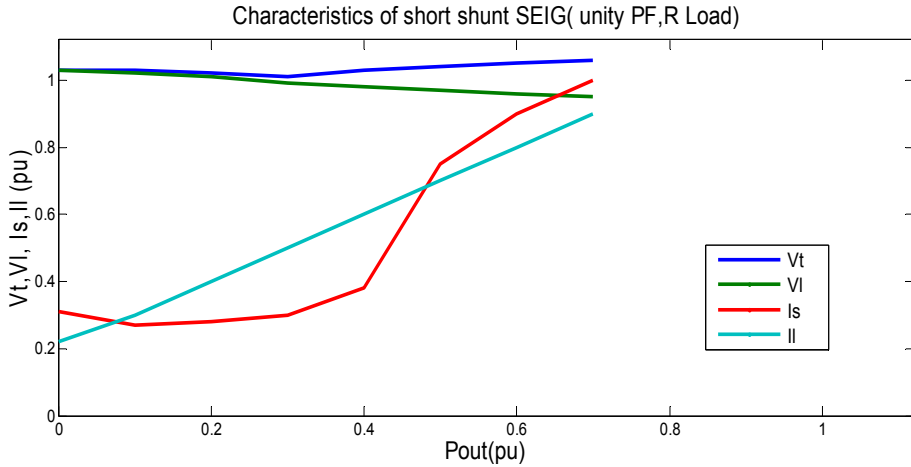
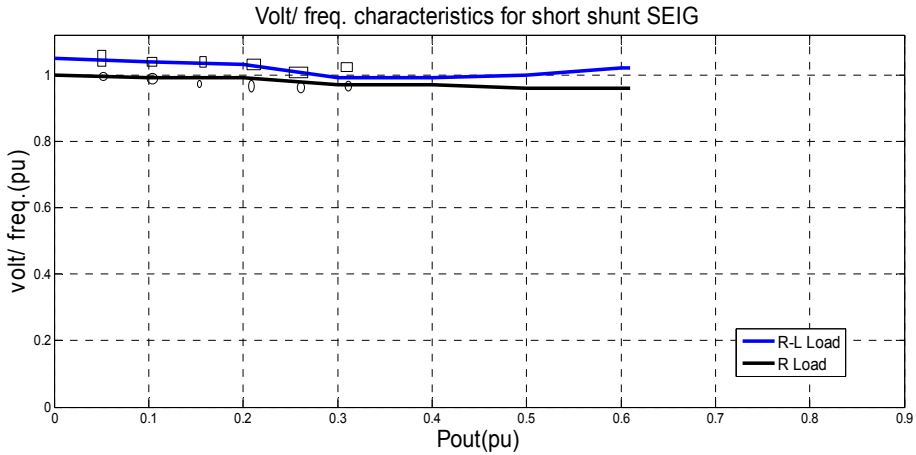


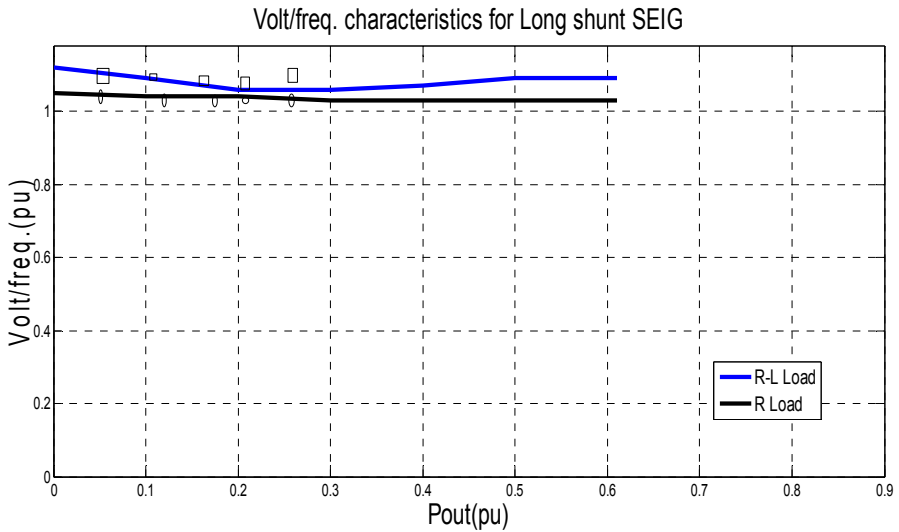
Figure 6 represents the volt/freq. characteristics of SEIG in different loading conditions. The  $V/f$  characteristics show that  $V/f$  ratio is maintained at almost unity and almost constant for the whole loading range in  $R$ -load. In contrast, in the case of  $R-L$  load, it is more than unity and slightly decreases at around  $0.3 pu$  due to an increase in saturation level, and it again increases gradually with the increase in load.

**Figure 6** Volt/ freq. characteristics for short shunt SEIG (see online version for colours)



Similarly, in the long shunt configuration,  $C_{sse}$  is kept equal to 0. From Figure 7, it has been concluded that the optimum point is obtained at  $1.12 pu$  and  $1.26 pu$  in  $R$ -load and  $R-L$  load, respectively. The characteristics are the same for  $C_{sh} = 32.28 \mu f$  and  $C_{lse} = 198.47 \mu f$  in Figure 7. It has also been observed that the no-load terminal voltage is approximately  $1.1 pu$ . With the inclusion of higher values of  $C_{lse}$ , overloading capacity is increasing.

**Figure 7** Volt/ freq. characteristics for long shunt SEIG (see online version for colours)



The performance characteristics of the long shunt SEIG in Figure 8 also show that at no load,  $V_t$  and  $V_l$  maintain an equal voltage of  $1.1 \text{ pu}$ . With the increase in saturation level,  $V_1$  becomes constant and the current increases from  $0.39 \text{ pu}$  to  $1.18 \text{ pu}$ . The fluctuation of the load voltage with output power is negligible, as seen in Figure 8. Furthermore, the addition of series capacitance increases the system's overload capability.

**Figure 8** Performance characteristics of long shunt SEIG (see online version for colours)

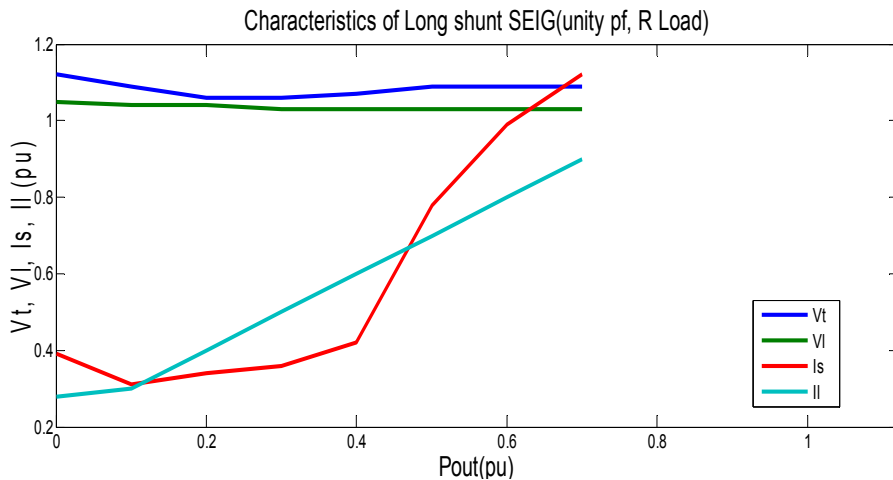


**Table 3** Comparative analysis of short shunt  $V/f$  ratio at a different power factor

<i>S. no</i>	$V/f$ (pu)	$P_{out}$ (pu) avg	Power factor
1.	0.98	0.95	Unity
2.	0.92	0.90	0.9
3.	0.89	0.85	0.8
4.	0.821	0.75	0.7

Tables 3 and 4 represent the comparative analysis of short and long-shunt SEIG at different power factors. Here, for Table 3, i.e., comparative flux analysis of short shunt SEIG, input parameters are  $C_{sh}=19.86 \mu f$ ,  $C_{sse}=200 \mu f$  and  $n=0.99 pu$ . Whereas for Table 4 long shunt analysis, input parameters are  $C_{sh}=24.21 \mu f$ ,  $C_{sse}=250 \mu f$  and  $n=0.82 pu$ . From the results, it has been concluded that at unity power factor, optimum  $V/f$  ratio or improved performance has been obtained. Also, higher values of capacitances are required for long-shunt connections compared to short-shunt connections.

**Table 4** Comparative analysis of long shunt  $V/f$  ratio at a different power factor

<i>S. no</i>	$V/f$ (pu)	$P_{out}$ (pu) avg	Power factor
1.	0.95	0.91	Unity
2.	0.90	0.89	0.9
3.	0.82	0.81	0.8
4.	0.71	0.72	0.7

#### 4.1 Effect of load ability

The optimum loadability of SEIG indicates its loading capability. Table 5 displays the findings of the short shunt SEIG design parameters for best loadability while feeding resistive and resistive–inductive loads. It has been observed from the table that optimum loading is achieved at  $1.07 pu$ ,  $13.22 \mu f$  and  $400.1 \mu f$  for R-load and correspondingly at  $0.98 pu$ ,  $25.64 \mu f$  and  $285.5 \mu f$  for R-L load. For a resistive load, the optimal point is attained at a prime mover speed 9.4% greater than the rated speed and low shunt capacitance. Unlike resistive loads, the optimal point for R–L loads is at 2.3 % lower prime mover speed than the rated speed with sufficient greater shunt capacitance.

**Table 5** Summary of optimum loadability for short shunt SEIG

<i>Configuration</i>	$Speed(n)$ (p.u)	$C_{sh}$ ( $\mu F$ )	$C_{sse}$ ( $\mu F$ )	$P_{out}$ (Pl) (p.u)	<i>Remark</i>
Short Shunt (PPA Algorithm)	1.07	13.22	400.1	0.999	R-Load
	1.0	16.89	447.5	0.941	
	0.98	25.64	285.5	0.907	R-L
	1.01	22.76	314.6	0.901	Load

For *R*- and *R-L* loads, the variation of *VI* and *II* for optimum loadability at rated speed is shown in Figure 9. *VI* remains nearly flat up to 0.79 *p.u* loading for resistive load and decreases below *Vl<sub>mn</sub>* beyond this loading. The voltage changes with *R-L* load are not smooth, as it drops from 1.03 to 0.9423 *p.u* at first and then rises to 1.062 *p.u* with load. Beyond 0.9 *p.u* loading the *V<sub>mx</sub>* is violated.

**Figure 9** Characteristics of optimum loadability for short shunt SEIG (see online version for colours)

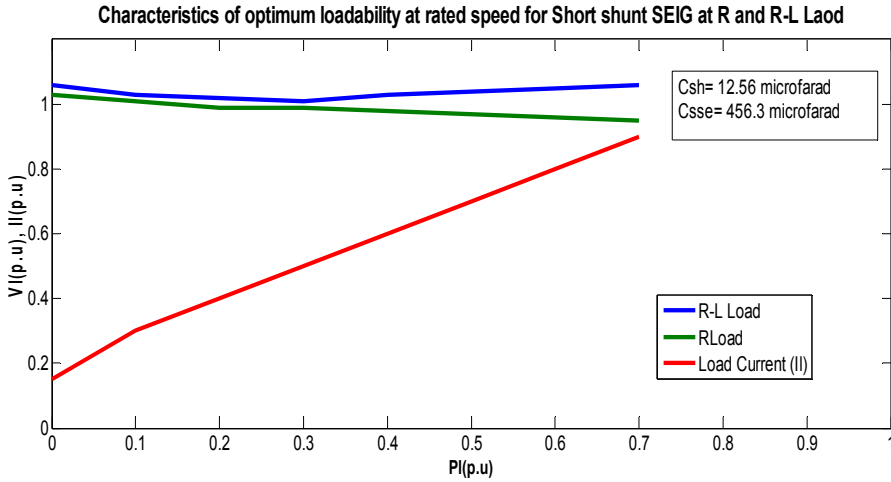
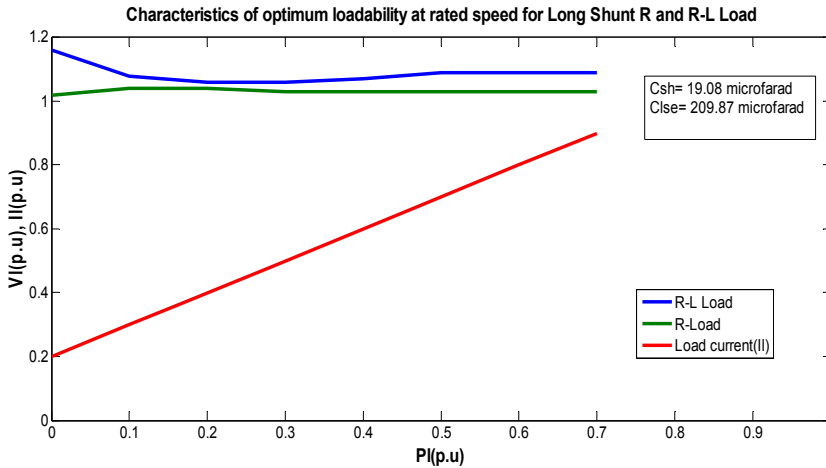


Table 6 displays long shunt SEIG design parameters, and it has been noticed that the optimum loading point is achieved at 1.02 *p.u* , 16.25  $\mu F$  , 421.0  $\mu F$  for *R*-load and 0.97 *p.u*, 23.5  $\mu F$  , 436.2.5  $\mu F$  for *R-L* load. Similarly, Figure 10 represents the variation of *VI* and *II* for long shunt SEIG at 19.08  $\mu F$  shunt capacitance and 209.87  $\mu F$  series capacitance. It has been observed from the figure that *VI* decreases from 1.13 *p.u* and further increases for *R-L* load, whereas for *R*-load *VI* is nearly flat.

**Table 6** Summary of optimum loadability for long shunt SEIG

Configuration	Speed ( <i>n</i> ) ( <i>p.u</i> )	<i>C<sub>sh</sub></i> ( $\mu F$ )	<i>C<sub>sse</sub></i> ( $\mu F$ )	<i>P<sub>out</sub></i> ( <i>Pl</i> ) ( <i>p.u</i> )	Remark
Long Shunt (PPA Algorithm)	1.02	16.25	421.0	0.98	R-Load
	0.99	21.64	441.2	0.95	
	0.97	23.5	436.2	0.904	R-L Load
	1.0	27.8	355.6	0.901	

**Figure 10** Characteristics of optimum loadability for long shunt SEIG (see online version for colours)

## 5 Conclusions

In this paper, a steady state model of SEIG has been developed for the improvement of  $V/f$  regulation and improving loadability of the machine. The optimised value of shunt and series capacitance has been selected using the PPA heuristic approach, which exhibits the properties of a strawberry plant. Several noticeable results have been summarised as follows:

- The  $V/f$  ratio, output power, and fitness for short shunt SEIG are better than the long shunt configuration, shown in Tables 1 and 2.
- In long shunt SEIG, an appropriate drop in terminal voltage has been observed, and hence it has unwanted oscillations. But it has the advantage of being easy to generate rated power at unity power factor.
- It has also been observed from Tables 3 and 4 that short shunt and long shunt configurations performed better at unity power factor with a per unit speed of 1.01 and 1.03  $p.u$ , respectively
- From Table 5 and 6, the optimum loading point has been achieved, which depicts the loading capacity of the SEIG machine. It has been observed that the optimum point is obtained at a prime mover speed of 9.4% greater than the rated speed and at a low shunt capacitance value.

Hence in this paper, the motive of improving flux requirement in SEIG and load capacity has been achieved with the help of the best possible PPA runners. Each iteration will lead to certain outcomes for the machine parameters. However, the PPA technique suffers from the shortcoming of being tested on low-dimension problems to establish its credentials. Finally, it could be concluded from this paper that in between the two configurations used, the short shunt is more suitable for the current SEIG machine. The

improved SEIG performance in WECS will lead to more wind energy conversion usage, especially for offshore areas. Hence, the increased usage of renewable energy will ultimately benefit society. Further research can explore the areas of effect of impedance loading on the SEIG efficiency, reliability & reduction in the size of the SEIG machine for remote locations of various mini- and micro-hydro plants.

## References

- Aberbour, A., Idjdarene, K. and Tounzi, A. (2020) 'Performance analysis of self-excited induction generator mathematical dynamic model with magnetic saturation, cross saturation effect and iron losses', *Mathematical Modelling of Engineering Problems. International Information and Engineering Technology Association*, Vol. 7 No. 4, pp.527–538.
- Almazini, H.F., Mortada, S., Hassan, F.A-A., Khraibet, H.N.A-B. and Alkenani, J. (2022) 'Improved discrete plant propagation algorithm for solving the traveling salesman problem', *International Journal of Artificial Intelligence (IJ-AI)*, Vol. 11, No. 1, pp.13–2.2.
- Al-Senaidi, A., Alolah, A. and Alkanhal, M. (2021) 'Modelling and effect of core loss in ac three phase self-excited induction generator used in wind energy applications', *Control and Operation of Grid Connected Wind Energy System: Green Energy and Technology*, Vol. 3, No. 2, pp.1–33.
- Aly, A., Aziz, A., Hamdy, R.A. and Khalik, A. (2019) 'Design and performance evaluation of a three phase SEIG feeding single phase loads', *Electric Power Components and Systems*, pp.1–16.
- Benhacine, T.Z-E., Nesba, A., Mekhtoub, S. and Ibtouen, R. (2021) 'Low-cost three-phase self-excited induction generator for supplying isolated single-phase loads', *International Journal of Digital Signals and Smart Systems*, Vol. 5, No. 1, pp.80–102.
- Bouhadjra, D., Kheldown, A. and Zemouche, A. (2020) 'Performance analysis of standalone six phase induction generator using heuristic algorithms', *Proceedings of the International conference on Emerging and Renewable Energy: Generation and Automation*, Elsevier, Vol. 167, No. C, pp.231–249.
- Chaturvedi, Y. (2022) 'Effects of magnetization characteristics on the performance of self-excited induction generator under unbalanced operations', *International Journal of System Assurance Engineering and Management*, Vol. 13, pp.375–384.
- Chaturvedi, Y. and Goel, A. (2019) 'Wind powered electricity generation through self-excited induction generator', *International Journal of World Scientific News*, Vol. 121, pp.90–100.
- Chaturvedi, Y., Kumar, S. and Gupta, V. (2020) 'Capacitance requirement for rated current and rated voltage operation of SEIG using whale optimization algorithm', *Proceedings of the International Conference on Computational Intelligence and Data Science (ICCIDS)*, Elsevier, Vol. 167, pp.2581–2589.
- Dewangan, S., Dyanamina, G. and Kumar, N. (2019) 'Performance improvement of wind-driven SEIG using Fuzzy logic controller', *International Transactions on Electrical Energy Systems*, Vol. 29, No. 8, pp.1–20.
- Esmeel, M.A. (2020) 'Steady state analysis of a wind energy driven self-excited induction generator', *Proceedings of the 8th IEEE International Conference on Smart Grid (IC smart grid)*, *International Journal of Renewable Energy Research*, Paris, pp.101–108.
- Esquivel-Sancho, L.M., Pereira-Arroyo, R. and Muñoz-Arias, M. (2021) 'Voltage regulation for a self-excited induction generator', *Proceedings of the 60th Institute of Electrical and Electronics Engineers Conference on Decision and Control (CDC)*, IEEE, USA.
- Hannan, M.A., Ali, J.A., Mohamed, A. and Hussain, A. (2018) 'Optimization techniques to enhance the performance of induction motor drives: a review', *Renewable and Sustainable Energy Reviews*, Vol. 2, pp.1611–1626.

- Kalla, U.K., Praveen, K., Agarwal, K.L., Sanjeev, S. and Shailendra, K. (2021) 'A state of art and comprehensive study of renewable energy systems based on three-phase self excited induction generator feeding single phase loads', *International Conference on Sustainable Energy and Future Electric Transportation (SEFET)*, Vol. 14, No. 18.
- Khan, F., Khan, R. and Iqbal, A. (2017) 'Modelling, implementation and analysis of a high (six) phase self-excited induction generator', *Journal of Electrical Systems and Information Technology*, Vol. 156, pp.1–18.
- Khan, M.F., Khan, M.R. and Iqbal, A. (2022) 'Effects of induction machine parameters on its performance as a standalone self-excited induction generator', *Energy Reports*, Vol. 8, pp.2302–2313.
- Krishna V.B.M. and Sandeep, V. (2022) 'Experimental investigations on loading capacity and reactive power compensation of star configured three phase self excited induction generator for distribution power generation', *Distributed Generation and Alternative Energy Journal*, Vol. 37, No. 3 pp.725–748.
- Mohiudin, R. and Sharma, P. (2021) 'Performance evaluation of a self-excited induction generator for stand-alone wind energy conversion system', *International Journal of Scientific Research and Engineering Trends*, Vol. 7, No. 5, pp.2391–2396.
- Paliwal, S., Sinha, S.K. and Chauhan, Y.K. (2019) 'Gravitational search algorithm-based optimization technique for enhancing the performance of self-excited induction generator', *International Journal of System Assurance Engineering and Management*, Vol. 10, pp.1082–1090.
- Saha, S.K. and Sandhu, K.S. (2018) 'Optimization techniques for the analysis of self-excited induction generator', *Proceedings of the 6th International Conference on Smart Computing and Communications ICSCC*, Elsevier, Vol. 125, pp.405–411.
- Salhi, A. and Eric, F. (2017) 'Nature-inspired optimization approaches and the new plant propagation algorithm', *Proceeding of the International Conference on Numerical Analysis and Optimization (ICeMATH2011)*, Yogyakarta, Indonesia, Vol. K2, pp.1–8.
- Satpathy, A.S., Kastha, D. and Kishore, N.K. (2019) 'Control of STATCOM assisted self-excited induction generator-based wind energy conversion system', *Institute of Electrical Technology (IET)*, pp.1904–1909.
- Sulaiman, M., Salhi, A., Khan, A., Mohammad, S. and Khan, W. (2018) 'On the theoretical analysis of the plant propagation algorithms', *Mathematical Problems in Engineering*. Doi: 10.1155/2018/6357935
- Teng, K., Lu, Z., Long, J., Wang, Y. and Roskilly, A.P. (2019) 'Voltage build-up analysis of self-excited induction generator with multi-time scale reduced-order model', *Institute of Electrical and Electronics Engineers*, Vol. 7, pp.48003–48012.
- Varshney, L., Vardhan, A.S.S., Vardhan, A.S.S., Kumar, S., Saket, R.K. and Kumar, P.S. (2021) 'Performance characteristic and reliability assessment of self-excited induction generator for wind power generations', *IET Renewable Power Generation*, Vol. 15, pp.1–19.

## Nomenclature

SEIG:	Self-Excited Induction Generator
IM:	Induction Machine
PM :	Prime Mover
PSO:	Particle Swarm Optimisation
PMSG:	Permanent Magnet Synchronous Generators
GA:	Genetic Algorithm
GSA:	Gravitational Search Algorithm
DFIG:	Doubly Fed Induction Generator
SCIG:	Squirrel Cage Induction Generator
SA:	Simulated Annealing
MNRE:	Ministry of New and Renewable Energy
NIWE:	National Institute of Wind Energy
PPA:	Plant Propagation Algorithm
WECS:	Wind Energy Conversion System
$C_{sh}$ :	Shunt capacitance ( $\mu F$ )
$C_{lse}$ :	Series capacitance for long shunt ( $\mu F$ )
$C_{sse}$ :	Series capacitance for short shunt ( $\mu F$ )
$V_t$ :	Terminal voltage in per unit

## Appendix A

### A.1: Induction machine parameters

Three phase, 3 kW, 415 V, 10.2A (line).  $R_s=0.072pu$ ,  $R_r=0.018pu$ ,  $X_{muns}=3.41pu$ ,  $0.65 \leq X_m \leq 1.32pu$

$$V_g = 1.53 - 0.29 X_m ; X_m < 1.48$$

$$V_g = 2.02 - 1.104 X_m + 0.44 X_m^2 - 0.066 X_m^3 ; 1.4 < X_m < 3.48$$

### Prime-mover parameters

Three phase, 10 kVA, 1500 rpm shunt motor.

### A.2: Coefficient of $Z$ total

The coefficients  $P$  and  $Q$  are defined as:

$$P1 = -X1RL(X2 + Xm) - X2RLXm$$

$$P2 = X1RLv(X2 + Xm) + X2RLXmv$$

$$P3 = R1R2RL + X1XcR2 + (R1Xc + RLXc)(X2 + Xm) + R2XmXc$$

$$P4 = ((-vR1Xc) - vRLXc)(X2 + Xm)$$

$$Q1 = 0$$

$$Q2 = X1RLR2 + (X2 + Xm)(R1Xc + RLXc) + XmR2RL + XmXcX2$$

$$Q3 = (X2 + Xm)(-R1RLv - X1Xcv)XmXcX2v$$

$$Q4 = -RLXcR2 - R1R2Xc$$